Journal of Catalysis 279 (2011) 276–286

Contents lists available at ScienceDirect

Journal of Catalysis

journal homepage: www.elsevier.com/locate/jcat

Hydrodeoxygenation pathways catalyzed by MoS_2 and NiMoS active phases: A DFT study

C. Dupont, R. Lemeur, A. Daudin, P. Raybaud *

IFP Energies Nouvelles, Direction Catalyse et Séparation, Rond-point de l'échangeur de Solaize, BP 3 – 69360 Solaize, France

ARTICLE INFO

Article history:
Received 3 December 2010
Revised 19 January 2011
Accepted 22 January 2011
Available online 4 March 2011

Keywords:
Hydrotreatment catalysts
MoS_2
NiMoS
Hydrodeoxygenation
Density functional theory
Nucleophilic substitution
Reaction pathway

ABSTRACT

Due to the increasing need for purifying renewable feeds (such as biomass effluents) by means of catalytic hydrotreatment processes, the atomic-scale understanding of the catalytic properties of transition metal sulfide active phases in the presence of oxygenated molecules becomes crucial. Using density functional theory (DFT) calculations, we evaluate the adsorption properties and the hydrodeoxygenation pathways of relevant model O-containing molecules on the M-edge sites of the MoS_2 and NiMoS active phase. We show first that the adsorption energies of methyl propanoate, propanoic acid, propanal, propanol and water are stronger on MoS_2 than on NiMoS. The interaction with the accessible Mo site is directed by the oxygen atom of either the C═O group for ester and acid or the OH group for alcohol and water molecules. For propanal, the adsorption mode depends on the nature of the active site: it is found to be bidentate on NiMoS, where the C and O atoms of the carbonyl group simultaneously interact with the dual Ni—Mo sites of the M-edge. The investigation into hydrodeoxygenation pathways reveals how the C═O hydrogenation and the C—O bond cleavage occur on transition metal sulfides. The specific adsorption mode provides a lower activation energy for the hydrogenation of propanal into propanol on NiMoS than on MoS_2. The propanol is further deoxygenated by a nucleophilic substitution mechanism involving a sulfhydryl group and leading to a thiol intermediate before propane formation. The rate-limiting step of the aldehyde HDO process is determined by the C—O bond cleavage step for which the activation energy is found smaller for NiMoS than for MoS_2.

1. Introduction

The decrease in available fossil fuel resources induces an increasing interest for alternative and renewable solutions, like the use of biomass. Hence from 2010, European Union imposes the introduction of 5.75% of renewable fuels extracted from biomass in fuels [1]. This kind of renewable sources of energy allows reduction in greenhouse gas emission compared to fossil fuels. Nevertheless, due to their high content in oxygenated compounds, the biomass effluents also present some disadvantages, like high viscosity, immiscibility to standard fuels or poor heating value. Hence, reducing the oxygen content is required to make bio-oils valuable for fuels. One possible solution is provided by the hydrodeoxygenation (HDO) route, which leads to the removal of oxygen atoms in the presence of hydrogen. The process may be rather similar to conventional hydrotreating, and existing refining processes can be used for the co-treatment of biomass effluents and petroleum fractions [2–5]. From the catalytic point of view, MoS_2-based catalysts promoted by either Co or Ni well known to be active in hydrodesulfurization (HDS) are also active in HDO (as described below). Moreover, the hydrotreatment of biomass effluents such as vegetable oils leads to paraffinic diesel, which exhibits properties close to conventional diesels. However, the HDO mechanism (including C═O hydrogenation and C—O bond cleavage) on MoS_2-based active phase remains unknown. At the same time, the hydrogen consumption induced by HDO processes makes crucial to better understand the HDO mechanisms taking place on such catalysts, subject of the present report.

According to previous experimental studies [6–8], complete hydrodeoxygenation occurs through three proposed routes: hydrodeoxygenation (HDO), decarbonylation and/or decarboxylation, producing H_2O, CO and CO_2, respectively, together with the targeted hydrocarbon compounds. The selectivity between the HDO route and the decarbonylation/decarboxylation one is governed by the relative easiness for breaking C—O bond versus C—C bond. These different pathways have been proposed for different kinds of oxygenated compounds, both aromatic derived from lignocellulosic biomass [4] and aliphatic derived from esters, acids or alcohols [7,8]. Concerning aliphatic esters, which are the major component of vegetable oils, Krause and coworkers have recently published experimental works [7–9] to investigate their transformation mechanisms on alumina-supported Co- and Ni-promoted MoS_2 catalysts. According to their studies, one key intermediate

* Corresponding author. Fax: +33 4 37 70 20 66.
E-mail address: pascal.raybaud@ifpen.fr (P. Raybaud).

0021-9517/$ - see front matter © 2011 Elsevier Inc. All rights reserved.
doi:10.1016/j.jcat.2011.01.025

for the selectivity between the HDO and the decarbonylation/decarboxylation routes proposed to be the aldehyde. Given its high reactivity, this interesting intermediate cannot be detected in high amounts, which makes difficult to understand its precise role during the HDO pathways. Moreover, aldehydes are also known to be present in various sources of biomass effluents [6], which encourages DFT studies of the reactivity of such molecules.

During the last decade, the atomic-scale description of the active sites present on MoS_2-based catalysts has made tremendous progress, thanks to the insights into density functional theory (DFT) simulations [10–13] but also cutting edge techniques as scanning tunneling microscopy [14,15]. This improved rational understanding of the local structure of the so-called CoMoS or NiMoS active phases has given the opportunity to investigate the complex hydrodesulfurization mechanisms involving relevant sulfur compounds as thiophene [16], thiols [17] or dibenzothiophene [11]. In contrast, DFT studies devoted to reaction mechanisms involving oxygen-containing molecules catalyzed by transition metal sulfides (TMS) are still scarce. For instance, two recent DFT studies have been recently published on water–gas shift reactions [18] and on the adsorption of furan compounds on MoS_2 edge active sites [19], while no DFT investigations have been performed on aliphatic oxygen-containing molecules to elucidate their hydrodeoxygenation mechanisms on Co(Ni)MoS catalysts. On the contrary, the reactivity of these molecules has been widely investigated theoretically on metallic surfaces [20–22]. Hence, the reactivities of the C═O, C═C, C—O and C—C bonds have been considered on different metals, either supported [23,24] or not [20,21]. In these studies, relevant aliphatic O-containing molecules have been considered: mainly alcohols, aldehydes and acids. In contrast to the observations made on TMS, the decarbonylation/decarboxylation route is known to be significantly predominant on metals [24].

The present study is devoted to the understanding of the reactivity of transition metal sulfide catalysts toward O-containing molecules by taking a specific attention to the hydrodeoxygenation routes. For that purpose, we focus on the active M-edge sites of the promoted NiMoS and non-promoted MoS_2 and make a coherent analysis of the chemical behavior of model O-containing molecules relevant for biomass deoxygenation (including vegetable oils). In the first part, the relative stability of relevant intermediates involved in the transformation of methylpropanoate is investigated on the M-edge sites of NiMoS and MoS_2. Then, starting from propanal suspected to be a relevant intermediate to explore HDO reactions (including C═O hydrogenation followed by C—O bond cleavage), a detailed mechanistic study is furnished on the Ni-promoted in comparison with the non-promoted MoS_2 active phases.

2. Methods

Periodic density functional theory calculations are performed using the VASP code [25,26]. General gradient approximation with PW91[27,28] for the exchange correlation functional and the projector augmented wave (PAW)[29] are used. The cutoff energy for the plane-wave basis is fixed to 500 eV, and the Brillouin zone integration is performed on a $(3 \times 3 \times 1)$ Monkhorst–Pack k-point mesh. The geometry optimization is completed when forces become smaller to the threshold of 0.03 eV $Å^{-1}$.

Periodic supercells of MoS_2 and NiMoS are modeled according to the results reported in numerous previous DFT studies [13,30–32] and more particularly the recent one for NiMoS by Krebs et al. [33]. Due to the sulfo-reductive conditions used for HDO reactions of (T = 250 °C and $p(H_2S)/p(H_2)$ = 0.01 or even lower [7,8]), a rather low chemical potential of sulfur is applied to the catalytic systems. For the M-edge of MoS_2, this environment stabilizes a sulfur coverage of 37.5%, corresponding to 3 S atoms per 4 Mo-edge atoms in the supercell (substrate shown in Fig. 1a and b), according to the previous DFT studies. Note that for the non-promoted catalyst, four MoS_2 units in the z direction (perpendicular to the edge) and four Mo atoms in the x direction (parallel to the edge) are considered. This model mimics the existence of a low S-vacancy concentration on the M-edge of MoS_2 as expected from experimental conditions and DFT calculations. Oxygenated molecules can thus interact with the sulfur-deficient Mo sites (Figs. 1a and b), while hydrogen atoms can interact either with Mo center to form hydridic species or with the S atom to form protonic species (sulfhydryl groups). For the NiMoS catalytic model, four molybdenum sub-surface layers are considered in z direction, covered by one mixed Ni—Mo metallic row (substrate shown in Fig. 1c). Given the HDO conditions, the chemical potential of sulfur imposes the existence of Ni and Mo atoms together on the M-edge to be consistent with the Krebs' results [33]. Hence, the stable state of the promoted M-edge used for this study corresponds to an edge promotion rate of 50%, with a so-called Ni—Ni—Mo—Mo pairing configuration and a sulfur coverage of 12.5% (one surface sulfur atom per 4 M-edge atoms in the supercell). The sulfur atom is located in a bridging position between two paired Mo atoms. Besides, each Mo atom is surrounded by one Ni atom. Oxygenated molecules can thus interact either with the sulfur-deficient Mo sites (Fig. 1a and b) or with the Ni sites, while hydrogen atoms can interact either with metal centers to form hydridic species or with the S atom to form protonic species.

The following parameters, x = 12.29 Å, y = 12.80 Å and z = 27.01 Å, are used for the supercell, which ensures a vacuum interlayer of 15.00 Å (in z direction) and is sufficient to avoid spurious interactions between two edges belonging to neighboring supercells. In this work, we focus on the metallic edge (M-edge) for both systems. We complementarily used the DMol3 package [34] to determine Hirshfeld charges [35] of relevant active sites and atoms in studied molecules.

Concerning the reactivity study, initial reaction pathways are constructed with a set of eight intermediate geometries, obtained by linear interpolation with a mixed internal and Cartesian coordinate system, using the CARTE suite [36]. The minimization of the reaction pathways and the search of the transition states (TS) are then mainly performed with quasi-Newton algorithm using the BFGS update, as implemented in the CARTE suite, combined, in some cases, with the climbing-image nudged elastic band method (CI-NEB) implemented in VASP [37,38]. Once an approximate structure is reached with these approaches, the refinement of the TS geometry is achieved by the minimization of the residual forces with a DIIS algorithm (quasi-Newton). Each stationary point of the reaction pathway is then characterized with a complete vibrational analysis. All reported transition states correspond to first-order saddle points characterized by a single imaginary frequency.

3. Results

3.1. Adsorption properties on NiMoS and MoS_2

As a preliminary study for the reactivity, we investigate here the adsorption properties of relevant O-containing molecules derived from the hydrodeoxygenation of methylpropanoate on the M-edge of MoS_2 and NiMoS: propanoic acid, propanal, propanol and water. Chemisorption of methylpropanoate was investigated in details on both catalysts, and only the most stable results are reported for the other compounds in Table 1.

Two adsorption modes, represented in Fig. 1, are obtained for methylpropanoate on MoS_2, depending on which oxygen atom interacts with the surface. Hence, adsorption through the oxygen of the carbonyl group (C═O – Fig. 1a) is clearly favored, with an

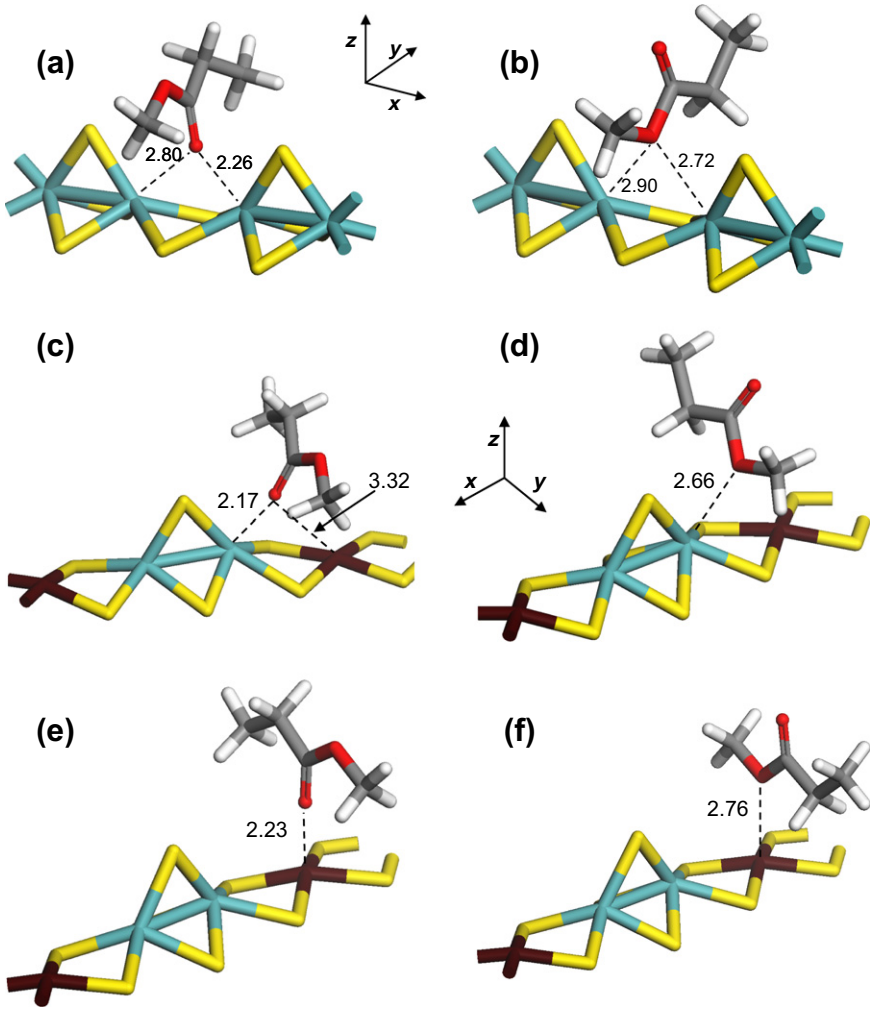

Fig. 1. Adsorption modes of methylpropanoate on MoS_2 and NiMoS, where the interaction takes place between: (a) C=O and 2 Mo sites of MoS_2, (b) C—O—C and 2 Mo sites of MoS_2, (c) C=O and Mo of NiMoS, (d) C—O—C and Mo of NiMoS, (e) C=O and Ni of NiMoS, (f) C—O—C and Ni of NiMoS. Relevant distances are reported in Å. *Color legend*: Mo is represented by blue sticks, Ni by brown sticks, S by yellow sticks, C by gray sticks, O by red sticks, H by white sticks. The same color legend is applied to all figures. (For interpretation of color in Figs. 1-12, the reader is referred to the web version of this article.)

Table 1
Adsorption energies (in eV) of methylpropanoate, propanoic acid, propanal and propanol on the M-edge of MoS_2 and NiMoS. Atoms of the slab directly involved in the chemisorption are reported as those of the molecule (in bold). The adsorption energy is defined as $E_{ads} = E(\text{slab + molecule}) - E(\text{molecule}) - E(\text{slab})$. A negative value corresponds to an exothermic adsorption process.

	Slab	Molecule	MoS_2	NiMoS
Methylpropanoate	Mo	C=**O**	−0.74	−0.43
	Mo	C—**O**—C	−0.33	−0.09
	Ni	C=**O**	–	−0.11
	Ni	C—**O**—C	–	−0.09
Propanoic acid	Mo	C=**O**	−0.65	−0.51
Propanal	Mo	C=**O**	−0.38	−0.43
	Mo—Mo	**C**=**O**	+0.02	–
	Mo—Ni	**C**=**O**	–	−0.66
Propanol	Mo	C—**O**	−0.83	−0.65
Water	Mo	H_2O	−0.76	−0.62

adsorption energy of −0.74 eV, compared to adsorption through the other oxygen atom (E_{ads} = −0.33 eV). This trend is assigned to the highest nucleophilic character of the oxygen of the C=O bond compared to that of the C—O—C group. Indeed, the oxygen of the carbonyl group obviously presents a more negative Hirshfeld charge (−0.26) than the oxygen of the ether group (−0.12). The same study is performed on NiMoS. Given the presence of the promoter, four adsorption modes may exist on this edge (Fig. 1).

According to adsorption energies reported in Table 1, chemisorption through the oxygen atom of the carbonyl group is also favored on NiMoS. Moreover, a clear preference appears for the interaction with Mo compared to Ni site. This can be explained by the higher electrophily of molybdenum sites compared to nickel sites, as shown by previous density of states analysis [13] and also evaluated by the Hirshfeld charges of the Mo (+0.33) versus the Ni (−0.07) sites.

In addition, for a similar adsorption site of the two catalysts, the interaction is greater with MoS_2 (−0.74 eV for the preferential site) than with the promoted catalyst (−0.43 eV). Although higher steric repulsions with sulfur atoms on the non promoted Mo edge are suspected, electronic effects seem to be predominant. According to the distances reported in Fig. 1, methylpropanoate interacts with two Mo atoms (each with a charge of +0.31) on MoS_2 in a asymmetric position, while it interacts with only one Mo site on NiMoS (the interaction with Ni being far less strong). Thus, this the combined contribution of the two electrophilic Mo atoms leads to a higher stabilization of the molecule on the MoS_2 M-edge.

Propanoic acid exhibits preferential adsorption modes very similar to those obtained for methylpropanoate. This molecule also

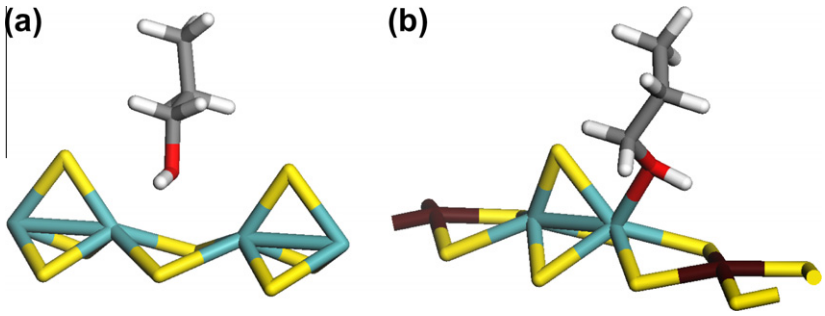

Fig. 2. Stable adsorption modes of propanol: (a) on MoS_2, (b) on NiMoS.

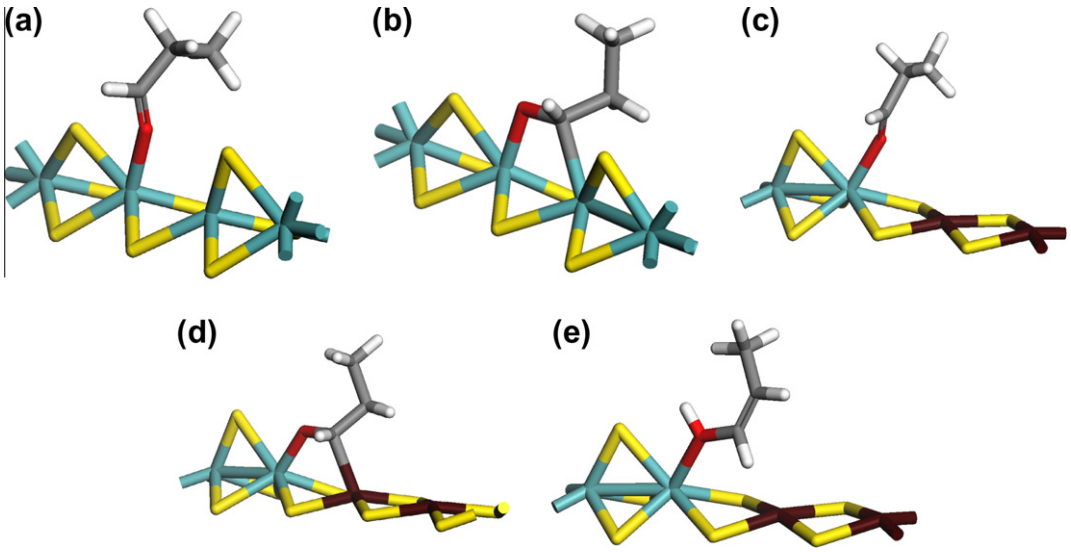

Fig. 3. Adsorption modes of propanal: (a) $\eta_1\mu_1$ on MoS_2, (b) $\eta_2\mu_2$ on MoS_2, (c) $\eta_1\mu_1$ on NiMoS, (d) $\eta_2\mu_2$ on NiMoS, and (e) enol form on NiMoS.

interacts with a Mo atom through the oxygen of the carbonyl. As for the ester molecule, adsorption energies (see Table 1) are greater on MoS_2 than on NiMoS.

Regarding propanol and water, both molecules exhibit high adsorption energies corresponding to an asymmetric bridging position between two Mo atoms on MoS_2 or to a single Mo–OHR interaction on NiMoS (Fig. 2). As for the ester and acid, the adsorption energies are stronger on the non-promoted system, which results from the two Mo site interactions. At this stage, it is also interesting to underline that the adsorption energies calculated for these O-containing molecules are higher than those reported for 2-methylthiophene on the same M-edge of NiMoS (−0.26 and −0.23 eV) and calculated with the same methodology [39]. This indicates that they may compete with sulfur compounds on the M-edge site and give rise to inhibiting effects.

Finally, preferential adsorption modes for propanal are reported in Fig. 3. One first contrasting behavior of propanal is that this molecule reveals a higher adsorption energy on NiMoS than on MoS_2. This energy trend is clearly explained by the specific adsorption mode of propanal found on NiMoS. Besides the metastable $\eta_1\mu_1$ mode with an O—Mo interaction found for the previous molecules (Fig. 3c), the $\eta_2\mu_2$ mode involving both an O—Mo and a C—Ni bond is stabilized on the M-edge of NiMoS (Fig. 3d) and the more favorable adsorption energy is −0.43 eV. This mode has also been tested on MoS_2 (Fig. 3b); however, it is metastable with an energy significantly higher than the $\eta_1\mu_1$ mode (Fig. 3a). For the CO molecule, it is well known that the bidentate adsorption mode is not stable versus a direct interaction with the C atom both on MoS_2 and on NiMoS [40]. Such a bidentate mode is thus specific of the aldehyde molecules adsorbed on NiMoS, while it is also known to be stabilized on metallic surface [22]. We have also tested the stability of the enol form of the propanal as suggested to be present by some experimental studies [3]. Actually, the energy level of the enol form as represented in Fig. 3e is about 0.65 eV less stable than the bidentate aldehyde, which means that this form is not favored on the catalytic edge.

Following this analysis on the specific adsorption of the aldehyde compound, we focus on the reactivity of propanal in the next section.

3.2. Reaction pathways

Following scheme proposed by previous experimental works [3,8], it seems reasonable to suggest that the aldehyde is first hydrogenated into propanol and then further deoxygenated into propane. It is thus a relevant model molecule to explore the C═O hydrogenation followed by the C—O bond breaking. Moreover, HDO is a rather preferred pathway on MoS_2-based catalyst [5]; hence, we investigate this pathway first on NiMoS and then compare it to MoS_2.

3.2.1. NiMoS catalyst

(a) Hydrogenation of propanal into propanol:

The reaction pathway to produce propanol is first considered. Starting from the coadsorbed state between propanal and dissociated hydrogen, two possible paths are reported in Fig. 4: CH

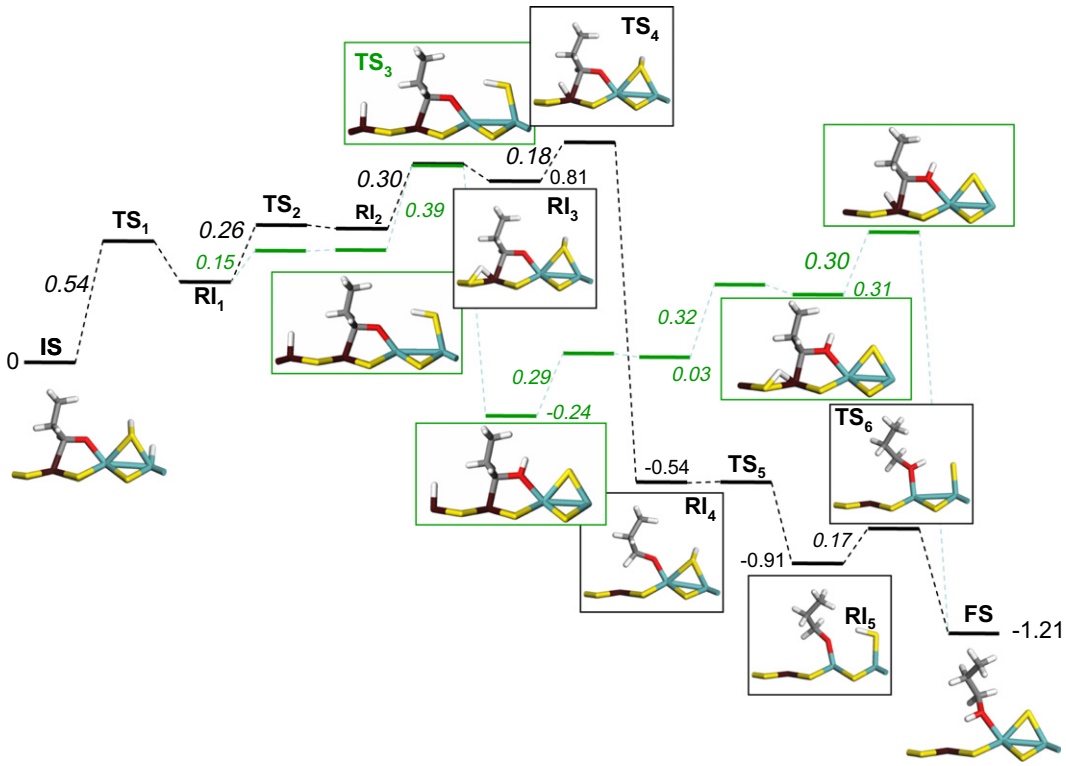

Fig. 4. The two possible hydrogenation pathways of propanal on NiMoS: the propoxy route with first CH and then OH formation (black); the hydroxylpropyl route with first OH and then CH (green). The most stable coadsorption state between propanal and two hydrogen atoms is taken as reference. IS corresponds to the initial state, TS_i indicates the transition state of step *i*, RI_i a reactional intermediate and FS the final state. Only, structures of initial, transition and final state of the two main steps (C—H and O—H formations) are reported, as well as the coadsorbed state taken as reference. (Energies are reported in eV.)

formation leading to the propoxy ($CH_3CH_2CH_2O$) intermediate followed by OH formation or OH formation leading to the hydroxypropyl (CH_3CH_2CHOH) intermediate followed by CH.

After dissociative adsorption of hydrogen in the presence of propanal, the preferential coadsorbed state corresponds to propanal adsorbed on its bidentate mode and hydrogen heterolytically dissociated on Mo and S (Fig. 4, **IS**). This most stable coadsorbed state is taken as reference. From this initial configuration, several activated steps for hydrogen diffusion are required to obtain the precursor state (Fig. 4, $\mathbf{RI_3}$) of propanal hydrogenation. These diffusion steps correspond to the transition states TS_1 to TS_3 with activation energy barriers of 0.26 and 0.54 eV. These values are consistent with previous DFT results [41,42].

We now analyze the key elementary acts leading to the propoxy intermediate. According to the propoxy route, the two successive monohydrogenation steps appear to be widely favored on a thermodynamic and on a kinetic point of view. Indeed, they are widely exothermic with ΔE(C—H) = −1.35 eV and ΔE(O—H) = −0.30 eV. For the kinetic aspect, despite the presence of coadsorbed hydrogen sharing a Ni atom, propanal remains in the bidentate mode in the precursor state $\mathbf{RI_3}$. Due to this coadsorption on the same nickel atom, hydrogen is chemisorbed in an asymmetric bridging position with d(S—H) = 1.45 Å and d(Ni—H) = 1.70 Å. Nevertheless, hydrogen remains in the vicinity of propanal, inducing a short *C···H* distance of 2.45 Å. This local configuration certainly acts in favor of the formation of the C—H bond. To reach the transition state, the bridging hydrogen is shifted to the nickel atom. Thus, in $\mathbf{TS_4}$, d(Ni—H) is decreased to 1.51 Å, while d(S—H) is elongated to 1.79 Å. The *C···H* distance is also shortened to 2.04 Å, associated with an elongation of i699 cm^{-1} along the active mode. According to this analysis, this transition state can be characterized as an early TS and is associated with a low activation energy barrier of 0.18 eV.

In order to initiate the second hydrogen transfer from the SH group to the O atom, it occurs a preliminary rotation of the SH fragment, combined to a rotation of the propoxy group. This non-activated reaction is exothermic with $\Delta E(\mathbf{RI_5}/\mathbf{RI_4})$ = −0.37 eV. The hydrogen atom is then transferred to lead to $\mathbf{TS_6}$ where the sulfur atom is on a Mo top position and propanol is almost formed on top of the second Mo atom. This transition state still presents a very low activation energy barrier of 0.17 eV associated with a vibration of i42 cm^{-1} along the active mode. In the final state (FS), the S atom recovers the bridging position and the propanol interacts with its O atom on the Mo atom in a tilted configuration.

The second possible route for propanal hydrogenation involves the O—H formation leading to the hydroxypropyl intermediate followed by the C—H formation (green[1] pathway in Fig. 4). In this sequence, the elementary acts are still widely exothermic, but they present higher activation energy barriers of 0.39 and 0.30 eV, respectively.

At this stage, it is interesting to compare our results with DFT kinetic data for metallic surfaces. For the palladium (1 1 1) surface, Pallassana and Neurock found that the propoxy route is thermodynamically preferred with a nearly isoenergetic C—H formation followed by an exothermic O—H formation [21]. On the platinum (1 1 1) surface, Alcala et al. showed that the DFT activation energy for the propoxy formation was about 0.4 eV, and for the subsequent alcohol formation, the value was about 0.15 eV [43]. Hence, given these reference results for metallic surfaces, NiMoS phase appears to be very efficient for propanal hydrogenation into propanol. Moreover, the fact that multiple monohydrogenation pathways are possible for aldehyde also makes this step statisti-

[1] For interpretation of color in Figs. 1–12, the reader is referred to the web version of this article.

cally easier and less constrained (this will not be the case for MoS_2 as discussed further).

It can be also noticed that for the hydrogen coverage assumed in the present study, the hydrogenation steps are kinetically competitive or even more favorable than hydrogen diffusion steps.

As a corollary, the previous section has shown that the enol form of propanal is about 0.65 eV higher in energy than propanal itself. Moreover, its formation requiring the transfer of one H atom from the —CH_2— group of CH_3CH_2CHOH to the edge is unfavored. Hence, if the propenol intermediate is formed, it is rapidly isomerized into the aldehyde form further hydrogenated into propanol.

(b) C—O bond breaking of propanol:

Once propanol is obtained, C—O bond splitting has to be considered to continue the HDO route. On Pt(1 1 1), Alcala et al. [20] proposed, as the first elementary act, a cleavage of the C—H bond to lead to a partial dehydrogenation of propanol. However, given the ability of propanal to be hydrogenated on NiMoS and given the hydrogen pressure in the reaction conditions, this reverse reaction appears to be unlikely. Moreover, considering values reported in Fig. 4, the splitting of the C—H bond of propanol to form C_2H_5CHOH is endothermic with ΔE = +1.39 eV. Thus, we propose to investigate the breaking of the C—O bond through the formation of thiol, which is suspected to be possible due to the presence of —S—H groups at the M-edge. A similar route was proposed experimentally for hydrodenitrogenation (HDN) of amines [44–47]. Moreover, during HDO of methylpropanoate, thiols have been observed by Senol et al. [8]. In such a nucleophilic substitution (S_N) scheme, the surface sulfhydryl group is directly involved to transform propanol into propanethiol, and then propane is obtained by hydrodesulfurization (HDS). The initial, transition and final states of this elementary act of C—O splitting are represented in Fig. 5.

This reaction is slightly exothermic (ΔE = −0.16 eV) and presents a relatively high activation barrier of +1.49 eV. Nevertheless, this barrier remains attainable. Given the structures represented in Fig. 5, the breaking of the C—O bond occurs through the formation of a transient primary carbocation interacting simultaneously with the hydroxyl and the sulfydryl groups as it occurs similarly during a nucleophilic substitution mechanism. This result is comparable to mechanisms previously proposed for HDN of aliphatic amines [44–47]. According to these experimental results, the thiol intermediate is produced during the HDN of primary amines and the final rate of alkene and alkane is determined by the thiol reactivity.

(c) Desulfurization of propanethiol:

The thiol desulfurization is the subsequent step toward hydrocarbon formation. From the coadsorbed state between propanethiol, OH and H species (RI_1 in Fig. 5), two forthcoming pathways may occur: either direct desulfurization (DS) in presence of the coadsorbed OH and H species followed by water desorption or water release followed by thiol DS.

Given the coadsorption mode of propanethiol, OH and H species, direct DS can occur only through an intramolecular mechanism combining the cleavages of the C—S and S—H bonds and C—H formation. The initial, transition and final states of this elementary step are represented by the black pathway in Fig. 5. This elementary act is characterized by a low exothermicity of −0.11 eV and especially a high activation energy of 2.18 eV. Hence, given this particularly high value, this pathway seems to be very unlikely to occur. Furthermore, in such a scheme, the C—S bond breaking appears to be the rate-determining step, compared to nucleophilic substitution involved in C—O bond cleavage. Such a trend would contradict with the chemical intuition for which the C—S bond breaking is less demanding than the C—O bond breaking. According to previous experimental studies on HDN, the thiol is supposed to be created relatively slowly but to be rapidly converted [47].

A second pathway (represented in green in Fig. 5) is investigated by assuming DS occurring after water elimination. Starting from propanethiol coadsorbed with the OH and H species (RI_1 in Fig. 5), the water formation is first investigated. Regarding the thermodynamic aspect, the formation of water presents an exothermicity of −0.23 eV, contrasting with the thiol DS isothermicity in the presence of coadsorbed OH and H. During this reaction, the

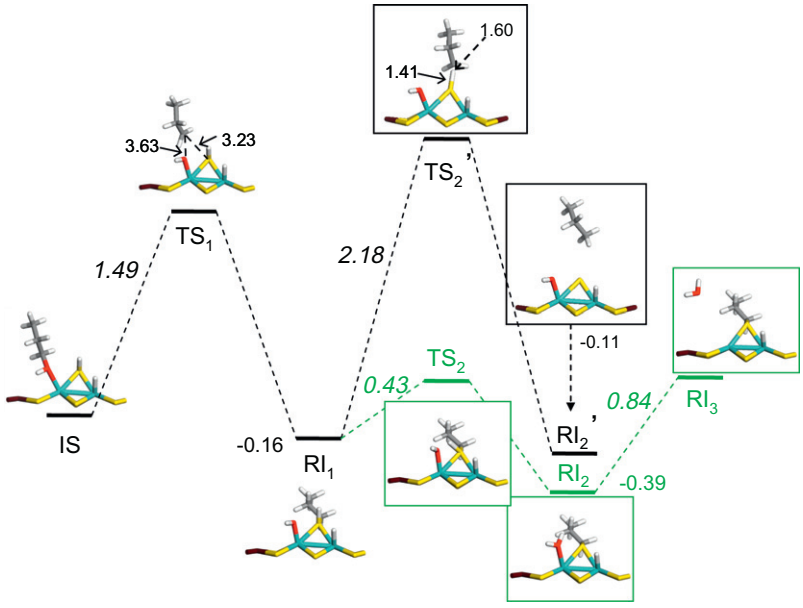

Fig. 5. Reaction pathways for the C—O bond breaking over NiMoS. Pathway represented in black: desulfurization of propanethiol followed by water desorption; pathway represented in green: water desorption followed by the thiol desulfurization step (represented in Fig. 6). Energies are reported in eV, and relevant distances are reported in Å.

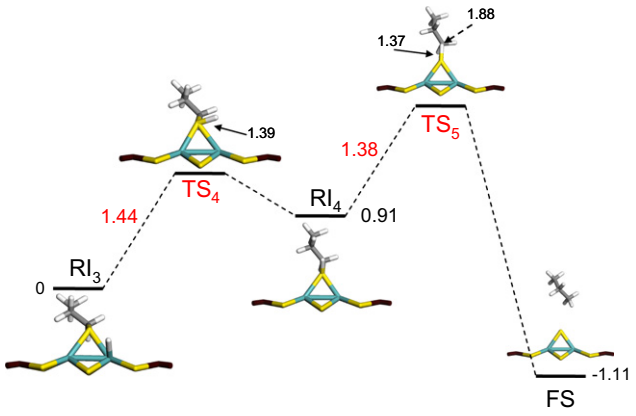

Fig. 6. Hydrogen migration followed by thiol desulfurization on NiMoS: initial (RI_3, in consistence with Fig. 5) and final state (FS), as well as the two transition states (TS_i) and the reactional intermediate (RI) are represented. Relevant energy distances are reported in eV and Å, respectively.

S—H fragment rotates toward OH to reach the TS corresponding to a moderate activation energy barrier of 0.43 eV. In the transition state, S—H is orientated in the same direction than O—H. The S—H bond is slightly elongated from 1.36 Å in the initial state to 1.49 Å, while the difference is more significant for the O—H bond between the transition state (d($O\cdots H$) = 1.45 Å) and the final state (d(O—H) = 0.98 Å). This is in agreement with the moderate activation energy barrier and thus an early TS. In the final state, the structure of adsorbed water is very close to that gas phase molecule. All attempts to localize a transition state demonstrate a non-activated process. Thus, desorption of water is defined only by its thermodynamic component which corresponds to an energy of 0.84 eV. To conclude about this whole process of water formation, the highest energy gap is due to the desorption of water. Up to this point, this barrier of 0.84 eV remains lower than the activation barrier involved in thiol DS in the presence of coadsorbed OH and H.

Starting from the final state of Fig. 5 (RI_3), after the removal of the water molecule, the next step consists of the hydrogen migration from Mo to S before the formation of propane. The complete pathway is represented in Fig. 6. The hydrogen migration from Mo to S is not thermodynamically favored with an endothermicity of 0.91 eV and accordingly a high activation barrier of 1.44 eV. The final step corresponding to an internal migration of H from S to CH_2 is much more favorable, especially concerning the thermodynamic aspect: DS is widely exothermic with $\Delta E = -2.03$ eV, associated with an activation energy barrier of 1.38 eV, which is significantly lower (−0.8 eV) than in the previous scenario. Thus, our study reveals that desorption of the water molecule is mandatory before the DS step.

As an intermediate conclusion, the previous study shows that the two less kinetically demanding monohydrogenation steps occur on the bidentate-adsorbed propanal and are activated by the Ni—H and the Mo—SH species. The rate-determining step of the process consists of the C—O bond breaking occurring through a nucleophilic substitution mechanism involving a sulfhydryl group in a bridging position between two Mo sites.

3.2.2. MoS_2 catalyst

In order to better understand the role of the promoter and in particular, the influence of the bidentate adsorption mode of propanal on NiMoS and not found on MoS_2, the hydrodeoxygenation mechanism of propanal is now investigated on the non-promoted catalyst.

(a) Hydrogenation of propanal:

The complete hydrogenation pathway of propanal is represented in Fig. 7, and both energetics and structures of intermediates and transition states are reported. In that case, we do not investigate H diffusion steps, subject of previous DFT works [48–50]. The corresponding activation energies for the diffusion steps can be as high as the one found on NiMoS (see previous paragraph). Hence, we start from the most stable coadsorption state between propanal and dissociated hydrogen which corresponds to the precursor state favorable for C—H and O—H bond formations. As for the promoted catalyst, hydrogenation is widely exothermic with the same critical steps: C—H ($\Delta E = -0.81$ eV) and O—H ($\Delta E = -0.51$ eV) formations, according to the propoxy route. The hydroxylpropyl route, namely O—H formation followed by C—H formation, has been investigated, but the hydroxylpropyl intermediate is not stabilized on the MoS_2 surface. Thus, only the propoxy route is discussed in what follows.

Starting from propanal coadsorbed with hydrogen dissociated over the neighboring Mo—S species, the formation of the C—H bond occurs first by the hydrogen transfer from the S—H group. In the transition state, the Mo—S(H) bond close to the propanal is shortened from 2.49 Å in the initial state to 2.27 Å in the TS, while the second Mo—S bond is elongated from 2.59 to 3.54 Å. In addition, the S—H rotates to optimize the $S\cdots H\cdots C$ structure in the TS, with d($C\cdots H$) = 1.42 Å and d($S\cdots H$) = 1.54 Å. The formation of this TS is associated with an activation barrier of 0.73 eV and an elongation frequency of i692 cm^{-1} along the active mode.

Once the propoxy intermediate is obtained, the next step consists in the formation of the O—H bond. Given the relative conformations of propanal (**RI_1**) and propanol, a rotation of the propyl chain occurs preliminary to the elementary act of O—H formation. This reaction is almost athermic ($\Delta E = -0.05$ eV) and presents a low activation barrier of 0.10 eV. This TS is characterized by a low imaginary frequency of i57 cm^{-1}, corresponding to the rotation of the C_2H_5 fragment.

For the formation of the O—H bond leading to propanol, the propoxy coadsorbed with hydrogen on Mo remains almost fixed in the bridging configuration, while hydrogen translates over the Mo—O bond. In the transition state where d($M\cdots H$) = 1.81 Å and d($H\cdots O$) = 1.46 Å, it is found an activation barrier of 0.84 eV and a frequency of i1328 cm^{-1} corresponding to the elongation of the O—H bond.

If we analyze the hydrogenation pathways of propanal on MoS_2 and on NiMoS, we notice that both paths are widely exothermic ($\Delta E = -1.37$ and -1.21 eV on MoS_2 and NiMoS, respectively), contrary to what occurs on metals. Alcala et al. [24] found that this reaction is slightly endothermic on Pt(1 1 1), with $\Delta E = +0.23$ eV. As previously underlined for NiMoS, this result confirms the high thermodynamic hydrogenating ability of sulfide catalysts even compared to metals. However, from a kinetic point of view, a key difference between MoS_2 and NiMoS is highlighted. On NiMoS, the two critical steps for C—H followed by O—H formations present very low activation energy barriers of 0.18 and 0.17 eV, respectively, whereas the corresponding barriers (0.73 and 0.84 eV, respectively) are much more important on MoS_2. Although these barriers are higher compared to NiMoS and metallic surfaces, propanal hydrogenation remains accessible on MoS_2. This higher hydrogenating ability of NiMoS is explained by the bidentate adsorption mode of propanal, which is not stable on MoS_2. This specific chemisorption mode has several consequences. First, on the geometrical aspect, in the initial state d($H\cdots C$) = 3.93 Å on MoS_2, instead of 2.45 Å on NiMoS. Hence, the formation of the C—H bond is clearly facilitated in this latter case. Moreover, the sequence of the reaction is also in favor of the promoted catalyst where the H transferred on O comes from a S—H fragment, while it comes from a

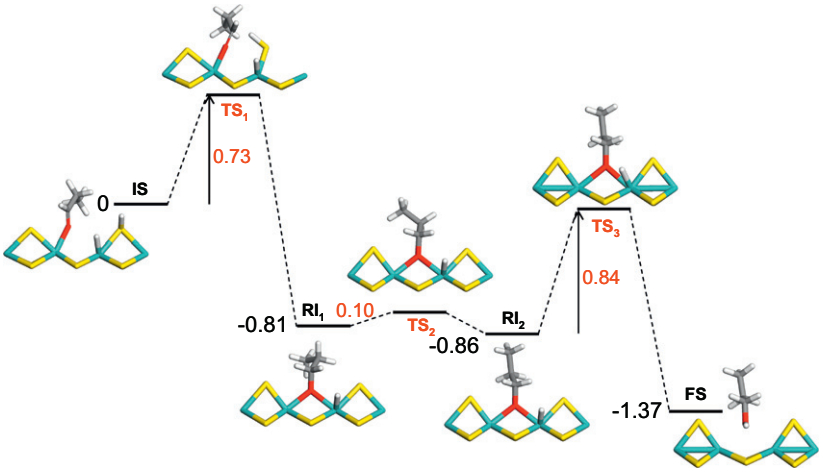

Fig. 7. Hydrogenation pathway of propanal on MoS_2. Energies are reported in eV; coadsorption of propanal with two hydrogen atoms is taken as reference. IS corresponds to the initial state, TS_i to the different transition states, RI_i to the reactional intermediates and FS to the final state. Activation energies and corresponding transition states are reported in red.

Mo—H fragment on MoS_2. The H—O distances are not affected in this case (d($H\cdots O$) = 2.42 and 2.31 Å on MoS_2 and NiMoS, respectively), but the strong difference in electronegativity between S and Mo modifies that of hydrogen (protonic in SH versus hydridic in Mo—H nature) and thus its affinity with oxygen. Moreover, the fact that one single hydrogenation route (propoxy) is possible on MoS_2 reduces from a statistical point of view, the number of reaction pathways on the non-promoted catalyst.

(b) C—O bond breaking of propanol:

As for NiMoS, we propose to follow the reaction pathway by considering a nucleophilic substitution of propanol in propanethiol. The initial, transition and final states of this elementary act are reported in Fig. 8. The detailed pathway is very similar to that on NiMoS. In the initial state, propanol is in its most stable configuration, coadsorbed with hydrogen atoms. This substitution is almost athermic with ΔE = +0.04 eV and is thermodynamically less favorable compared to NiMoS (−0.16 eV). Following a Brønsted–Evans–Polanyi principle, the activation energy barrier is higher than on the promoted catalyst: 1.76 instead of 1.49 eV. Despite these energetic differences, the geometrical evolution is similar to that observed on NiMoS.

(c) Desulfurization (DS) of propanethiol:

The two possible pathways, namely DS in the presence of OH and H, or DS preceded by water formation, are now investigated. The hydrodesulfurization pathway first considered in the presence of the coadsorbed species OH and H is reported in Fig. 9. This elementary act is more exothermic than on NiMoS: ΔE = −0.41 eV, instead of −0.11 eV. Nevertheless, the associated activation energy barrier is high: 2.04 eV. This value close to the one obtained on NiMoS is in agreement with the similar geometrical evolution and in particular with the identical d(S—H) and d(H—C) obtained for both transition states.

Given this high value obtained for DS in presence of coadsorbed H and OH, water desorption must be first considered following the pathway represented in Fig. 10. As for NiMoS, this path is divided into two parts: the formation of water followed by its desorption. The first step is very similar to the one obtained on NiMoS. In particular, the geometrical evolution characterized by the rotation of the SH fragment is identical to the one observed on the promoted catalyst. Besides, the two critical distances, S—H and $H\cdots O$, are identical at the transition state on both catalysts. This similar structural behavior is associated with equivalent energetics: an exothermicity of −0.37 eV and an activation energy barrier of

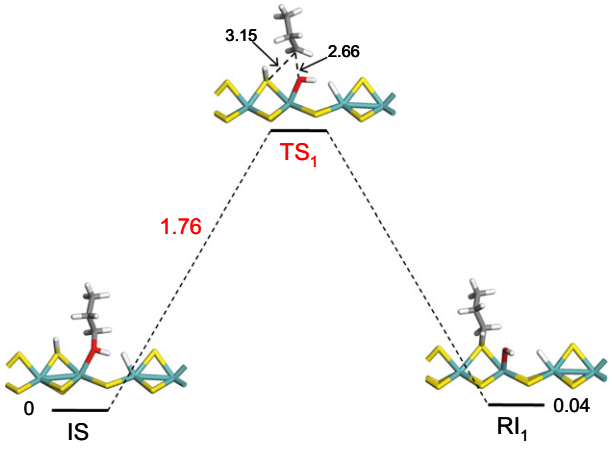

Fig. 8. Optimized structures of the initial state (IS), transition state (TS) and final state (RI_1) of the nucleophilic substitution of propanol. Energies are reported in eV, and characteristic distances in the transition state are given in Å.

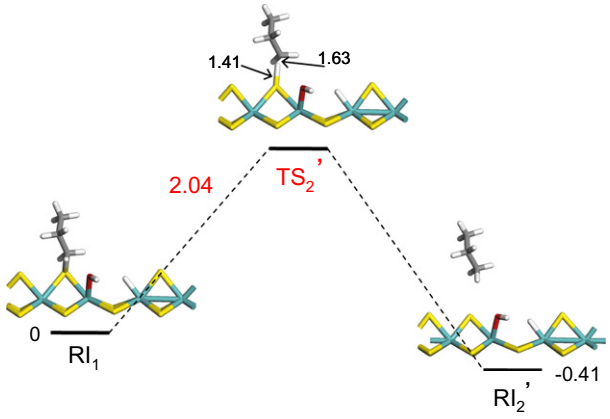

Fig. 9. Optimized structures of the initial state (RI_1), transition state (TS_2') and final state (RI_2') of the hydrodesulfurization of propanethiol. Energies are reported in eV, and characteristic distances in the transition state are reported in Å.

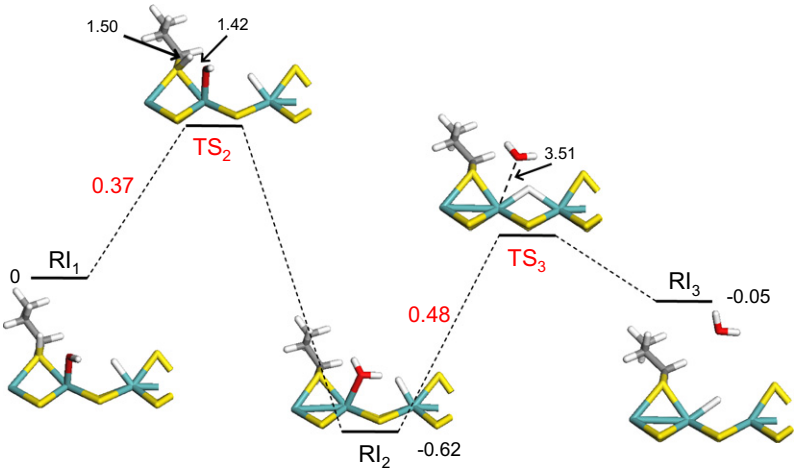

Fig. 10. Optimized structures of the initial state (RI_1, in agreement with Fig. 8), reactional intermediate (RI), transition states (TS_i) and final state (RI_3) of the formation of water on MoS_2. Activation energy barriers and characteristic distances in the transition states are reported in eV and in Å, respectively.

+0.37 eV. These values are consistent with the ones obtained on the promoted catalyst (−0.29 and +0.43 eV, respectively).

In contrast, the second elementary act differs more widely. On MoS_2, a transition state is localized for the desorption of water. As on NiMoS, this desorption is endothermic with ΔE = +0.33 eV, the corresponding activation energy barrier is equal to 0.48 eV. The differences observed compared to the promoted catalyst is linked to the vicinity of the hydrogen present in the vacancy. Hence, this hydrogen evolves from a top position over one of the molybdenum atom (see **RI₁** and **RI₂** in Fig. 10) to a near-bridge position (see **RI₃** in Fig. 10), while a real bridge position is observed at the transition state. Despite the activation energy barrier of water desorption, the direct pathway leading to the formation of water is widely favored over the desulfurization in presence of coadsorbed OH and H.

Finally, desulfurization of propanethiol is considered, without any coadsorbed species. The different key structures are reported in Fig. 11. Like on NiMoS, this path is composed by a first endothermic elementary act (ΔE_1 = +1.18 eV) corresponding to the migration of hydrogen, and by a second step, the desulfuration itself, widely exothermic (ΔE_2 = −1.72 eV). In the initial state, hydrogen is chemisorbed on top of a molybdenum atom. On MoS_2, the Mo—H bond is parallel to the Mo atomic edge raw, while it is perpendicular (see **RI₃** in Fig. 6) on NiMoS, which makes the hydrogen migration slightly more energy demanding. In the transition state, the S—H fragment is partially rotated and d(S—H) = 1.39 eV, like on the promoted catalyst. The associated activation energy barrier is equal to +1.58 eV. This value is slightly higher than on NiMoS (E_{act} = 1.44 eV). This trend is also consistent with the larger endothermicity calculated on MoS_2: 1.18 eV instead of 0.91 eV.

On the contrary, the desulfurization step of the thiol is widely exothermic (ΔE_2 = −1.72 eV) and the corresponding activation energy barrier is equal to 1.25 eV. From the geometric point of view, the transition state (**TS₅** in Fig. 11) differs to the one obtained on NiMoS (**TS₅** in Fig. 6). Only the length of the new *C···H* bond is identical. The S—H bond is slightly shorter, but the main difference comes from the S-bridging atom in the TS. On the promoted catalyst, the S atom is symmetrically located between the two Mo sites and the S—H bond is centered over this Mo_2SH fragment. On MoS_2, the Mo_2SH fragment is asymmetric with the Mo—S bond closer to the vacancy, 15% shorter than the second one. Besides, the S—H bond is no more centered and is orientated toward the vacancy.

The values obtained for this elementary step of thiol HDS without any coadsorbed species can be compared with previous theoretical results obtained by Todorova et al. [51], where HDS of CH_3SH and C_2H_5SH on MoS_2 edges have been studied for various sulfur coverage. For a similar sulfur coverage of the M-edge, the activation energy barrier for the methane formation was associated with an activation energy barrier of 0.83 eV and that of ethane with a barrier of 1.15 eV. Thus, the value of 1.25 eV obtained here

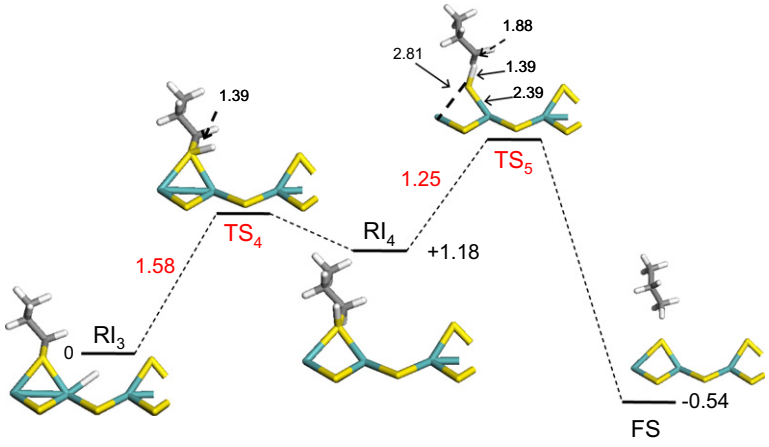

Fig. 11. Hydrogen migration followed by hydrodesulfuration on MoS_2: initial (RI_3, in agreement with Fig. 10) and final state (FS), as well as the two transition states (TS_i) and the reactional intermediate (RI) are represented. Energies and relevant distances are reported in eV and Å, respectively.

for propane not only is consistent with this previous study but reveals that the activation barrier for C—S bond cleavage increases with the aliphatic chain length.

4. Discussion

We compare the whole hydrodeoxygenation scheme on the two catalysts as reported in Fig. 12. In both cases, the hydrogenation of propanal is widely exothermic with low activation energy barriers. Moreover, the hydrogenation steps from propanal into propanol are kinetically favored over NiMoS versus MoS_2, which can be attributed to the bidendate adsorption mode of propanal involving the carbonyl group and both the Ni and Mo sites. The contribution of the mixed Ni—Mo site in the activation of the C=O double bond of propanal plays a key role for this step. The first monohydrogenation step involves the transfer of one hydrogen coming from the Ni—H species to the carbon of the carbonyl group leading to the propoxy intermediate. Due to the bidentate mode of adsorption of propanal, the carbon atom of the carbonyl and the Ni—H group are in close vicinity, which reduces the energy cost at the transition state. In addition, the hydroxylpropyl route is also competitive, which makes hydrogenation on NiMoS statistically more favorable.

In contrast, on the MoS_2 catalyst, the propanal is adsorbed in $\eta_1\mu_1$ configuration with the O atom on top of the Mo site. Only the propoxy route is possible and the first monohydrogenation involves the —SH group closer to the carbon of the carbonyl, whereas the hydrogen transfer from the Mo—H to the carbon of the carbonyl is sterically hindered. As a result, this step on MoS_2 is more kinetically demanding (+0.55 eV), and the pathway is statistically constrained. In addition, the second monohydrogenation step is even more favorable on NiMoS (by about 0.77 eV) due to the fact that the transfer occurs from the SH (protonic character) species to the O atom of the alkoxy species, which has high affinity for proton. On MoS_2, the source of hydrogen is now the Mo—H species (hydridic character), which is a less favorable situation. This result confirms the key contribution of mixte Ni—Mo sites located on the M-edge in the hydrogenation of C=O group of aldehyde. The trend revealed on NiMoS is rather close to the hydrogenation route of aldehyde investigated on metallic surface such as Pd(1 1 1) [20] and Pt(1 1 1) [21] where the di—σ bonding is also invoked and the alkoxy or hydroxylalkyl routes are both possible. In the case of NiMoS M-edge, this behavior is particularly due to the presence of the dual Ni—Mo site, which activates more easily the double bond of the carbonyl group. It is interesting to recall that the specific hydrogenating role of dual Co—Mo or Ni—Mo site located on the M-edge was also previously invoked for toluene hydrogenation of CoMoS [52] or olefin hydrogenation [39].

At this stage, the question of the selectivity between the hydrodeoxygenation and decarbonylation route can be qualitatively discussed, although it was not the purpose of the present study to address the mechanism of aldehyde decarbonylation. According to the scheme proposed by Senol et al. [8], the orientation toward C—C bond breaking might be induced by the aldehyde decarbonylation. Given the low calculated kinetic barriers of propanal to be hydrogenated into propanol, and in particular the easiness of the C—H formation, the cleavage of the C—C bond is expected to be far more kinetically demanding. Although this specific point requires a more detailed investigation (beyond the scope of the present study), we can qualitatively explain why the HDO route is observed to be predominant on NiMoS, when starting from the aldehyde intermediate and in absence of any hydrogen limitation.

Regarding the rate-determining step, it is clearly linked to the C—O bond breaking step of propanol. As reported in Fig. 12, it occurs via the nucleophilic substitution (S_N) of the OH group by the surface SH group followed by HDS of the thiol intermediate. This result also underlines the key role of sulfydryl groups for the HDO reactivity, as it was proposed for the transformation of aliphatic amines on TMS catalysts [44,45,47,53]. Our study also shows that keeping coadsorbed OH and H species on the same site of thiol leads to the high inhibiting effect on the desulfurization step of thiol. Hence, on both catalysts, formation and desorption of water must occur before hydrodesulfurization. The energy cost for the preliminary water release is not rate determining; however, one can suspect that this may impact the overall rate of the reaction. Among all these elementary steps – nucleophilic substitution, water formation, water desorption, hydrogen migration and finally hydrodesulfurization – the nucleophilic substitution appears to be the rate-determining step. Besides, this critical step presents a lower activation energy barrier on NiMoS: +1.49 eV instead of +1.76 eV on MoS_2. This trend is driven by the Brønsted–Evans–Polanyi principle also associated with a stronger interaction energy of propanol on MoS_2, which refrains the C—OH bond cleavage in the transition state (the C—O bond distance at the TS is smaller by almost 1 Å). Combining this result with the fact that the hydrogenation steps are favored on NiMoS, the whole process of propanal hydrodeoxygenation is thermodynamically and kinetically favored on NiMoS compared to MoS_2, which helps to elucidate the origin of the promoting effect for HDO.

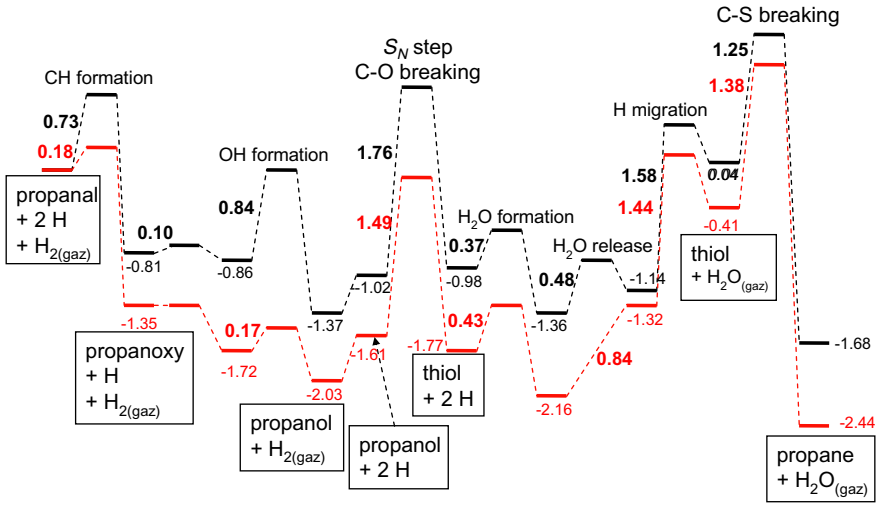

Fig. 12. Overall (simplified) hydrodeoxygenation pathway of propanal into propane over the NiMoS (red) and the MoS_2 (black) catalyst. The starting reference state is the proponal +2 hydrogen atoms in the precursor absorbed state before CH formation.

5. Conclusions

In summary, we have investigated by density functional theory, the adsorption properties and the reactivity of oxygenated molecules on the M-edges of MoS_2 and NiMoS. The model molecules have been chosen as being relevant of O-containing molecules (such as esters, acids, alcohols) present in biomass effluents to be hydrotreated before being incorporated into fuels. The adsorption energies of methyl propanoate, propanoic acid, propanol and water are exothermic and are slightly more favorable on MoS_2 than on NiMoS (by 0.14–0.31 eV). This trend is explained by the stable adsorption mode involving only the O atom interacting with one or two Mo sites depending on the system (promoted or unpromoted). In contrast, for the propanal molecule, the adsorption energy is more favorable on NiMoS than on MoS_2 (by 0.28 eV), which is due to the bidentate adsorption (di—σ) mode through the carbonyl group on the Ni—Mo mixte site. The aldehyde molecule appears as a thermodynamically stable intermediate during the HDO process of esters and carboxylic acids.

Moreover, the investigation into the mechanism for HDO of propanal reveals that the bidentate adsorption mode (similar to the one found on metallic surfaces) kinetically enhances its hydrogenation into propanol. This result may be seen as a manifestation of the synergy effect of mixed Ni—Mo sites present on the M-edge of NiMoS. Both the Ni and Mo sites contribute to the hydrogenation steps by activating the C and O atoms of the carbonyl group. Then, we found that the C—OH bond cleavage of the alcohol is activated by the sulfhydryl species present on both MoS_2 and NiMoS edges, which favors the nucleophilic substitution leading to the formation of thiol compounds followed by the desulfurization step. A similarity with nucleophilic substitution involved in the cleavage of the C—N bond of aliphatic amines was highlighted. The activation energy of the nucleophilic substitution step is lower on NiMoS than on MoS_2, which may be at the origin of the promoting effect of NiMoS in hydrodeoxygenation reaction.

Finally, we think that this work helps for a more rational understanding of the catalytic active transition metal sulfide phase with respect to HDO reactions. The present set of thermodynamic and kinetic data can also be used for building relevant microkinetic modeling of HDO reactions in the future.

Acknowledgments

The authors thank P. Fleurat-Lessard (ENS Lyon) to have kindly authorized the access to the CARTE software programmed with P. Dayal within the framework of SIRE (ANR-06-CIS6-014-04), a CNRS-ENS Lyon-IFP Energies Nouvelles joint project funded by the Agence Nationale de la Recherche (ANR). Calculations were performed with the IFP HPC and the authors are greatful to D. Klahr (IFPEN) for his technical help for VASP compilation. R. Lemeur thanks ISMANS for the teaching courses in the field of molecular modeling of materials.

References

[1] 2003/30/CE Directive, Official Journal of European Union, 2003.
[2] G.W. Huber, P. O'Connor, A. Corma, Appl. Catal. A: Gen. 329 (2007).
[3] B. Donnis, R.G. Egeberg, P. Blom, K.G. Knudsen, Top. Catal. 52 (2009) 229.
[4] A. Pinheiro, D. Hudebine, N. Dupassieux, C. Geantet, Energy Fuels 23 (2009) 1007.
[5] A. Daudin, T. Chapus, Prepr. Pap. – Am. Chem. Soc., Div. Petr. Chem. 54 (2) (2009) 122.
[6] E. Furimsky, Appl. Catal. A: Gen. 199 (2000).
[7] O.I. Senol, T.R. Viljava, A.O.I. Krause, Catal. Today 100 (2005) 331.
[8] O.I. Senol, E.M. Ryymin, T.R. Viljava, A.O.I. Krause, J. Mol. Catal. A: Chem. 268 (2007) 1.
[9] E.M. Ryymin, M.L. Honkela, T.R. Viljava, A.O.I. Krause, Appl. Catal. A: Gen. 358 (2009).
[10] P. Raybaud, Appl. Catal. A: Gen. 322 (2007) 76.
[11] J.-F. Paul, S. Cristol, E. Payen, Catal. Today 130 (2008) 139.
[12] L.S. Byskov, J.K. Nørskov, B.S. Clausen, H. Topsøe, J. Catal. 187 (1999) 109.
[13] P. Raybaud, J. Hafner, G. Kresse, S. Kasztelan, H. Toulhoat, J. Catal. 190 (2000) 128.
[14] S. Helveg, J.V. Lauritsen, E. Lægsgaard, I. Stensgaard, J.K. Nørskov, B.S. Clausen, H. Topsøe, F. Besenbacher, Phys. Rev. Lett. 84 (2000) 951.
[15] J.V. Lauritsen, J. Kibsgaard, G.H. Olesen, P.G. Moses, B. Hinnemann, S. Helveg, J.K. Nørskov, B.S. Clausen, H. Topsøe, E. Laegsgaard, F. Besenbacher, J. Catal. 249 (2007) 220.
[16] P.G. Moses, B. Hinnemann, H. Topsøe, J.K. Nørskov, J. Catal. 268 (2009) 201.
[17] T. Todorova, R. Prins, T. Weber, J. Catal. 246 (2007) 109.
[18] X.-R. Shi, S.-G. Wang, J. Hu, H. Wang, Y.-Y. Chen, Z. Qin, J. Wanga, Appl. Catal. A: Gen. 365 (2009) 62–70.
[19] M. Badawi, S. Cristol, J.-F. Paul, E. Payen, C. R. Chimie 12 (2009) 754.
[20] R. Alcala, M. Mavrikakis, J.A. Dumesic, J. Catal. 218 (2003) 178.
[21] V. Pallassana, M. Neurock, J. Catal. 209 (2002) 289.
[22] D. Loffreda, F. Delbecq, F. Vigné, P. Sautet, Angew. Chem. Int. Ed. 44 (2005) 5279.
[23] M.A.N. Santiago, M.A. Sanchez-Castillo, R.D. Cortright, J.A. Dumesic, J. Catal. 193 (2000) 16.
[24] K.I. Gursahani, R. Alcala, R.D. Cortright, J.A. Dumesic, Appl. Catal. A 222 (2001).
[25] G. Kresse, J. Hafner, Phys. Rev. B 47 (1993) 558.
[26] G. Kresse, J. Furthmüller, Phys. Rev. B 54 (1996) 11169.
[27] J.P. Perdew, Y. Wang, Phys. Rev. B 45 (1992) 13244.
[28] J.P. Perdew, J.A. Chevary, S.H. Vosko, K.A. Jackson, M.R. Pederson, D.J. Singh, C. Fiolhais, Phys. Rev. B 46 (1992) 6671.
[29] G. Kresse, D. Joubert, Phys. Rev. B 59 (1999) 1758.
[30] P. Raybaud, J. Hafner, G. Kresse, S. Kasztelan, H. Toulhoat, J. Catal. 189 (2000) 129.
[31] H. Schweiger, P. Raybaud, G. Kresse, H. Toulhoat, J. Catal. 207 (2002) 76.
[32] H. Schweiger, P. Raybaud, H. Toulhoat, J. Catal. 212 (2002) 33.
[33] E. Krebs, B. Silvi, P. Raybaud, Catal. Today 130 (2008) 160.
[34] B. Delley, J. Chem. Phys. 113 (2000) 7756.
[35] F.L. Hirshfeld, Theor. Chem. Acta B 44 (1977) 129.
[36] P. Dayal, P. Fleurat-Lessard, in preparation. Available at: http://perso.ens-lyon.fr/paul.fleurat-lessard/Carte.html.
[37] G. Henkelman, B.P. Uberuaga, H. Jonsson, J. Chem. Phys. 113 (2000) 9901.
[38] G. Henkelman, H. Jonsson, J. Chem. Phys. 113 (2000) 9978.
[39] E. Krebs, B. Silvi, A. Daudin, P. Raybaud, J. Catal. 260 (2008) 276.
[40] A. Travert, C. Dujardin, F. Maugé, E. Veilly, S. Cristol, J.-F. Paul, E. Payen, J. Phys. Chem. B 110 (2006) 1261.
[41] J.-F. Paul, E. Payen, J. Phys. Chem. B 107 (2003) 4057.
[42] M.Y. Sun, A.E. Nelson, J. Adjaye, J. Catal. 233 (2005) 411.
[43] R. Alcala, J. Greeley, M. Mavrikakis, J.A. Dumesic, J. Chem. Phys. 116 (2002) 8973.
[44] L. Vivier, V. Dominguez, G. Perot, S. Kasztelan, J. Mol. Catal. 67 (1991) 267.
[45] M. Cattenot, J.-L. Portefaix, J. Afonso, M. Breysse, M. Lacroix, G. Perot, J. Catal. 173 (1998) 366.
[46] Y. Zhao, P. Kukula, R. Prins, J. Catal. 221 (2004) 441.
[47] Y. Zhao, R. Prins, J. Catal. 229 (2005) 213.
[48] A. Travert, H. Nakamura, R.A. van Santen, S. Cristol, J.-F. Paul, E. Payen, J. Am. Chem. Soc. 124 (2002) 7084.
[49] M. Sun, A.E. Nelson, J. Adjaye, J. Catal. 233 (2005) 411.
[50] P.-Y. Prodhomme, P. Raybaud, H. Toulhoat, submitted for publication.
[51] T. Todorova, R. Prins, T. Weber, J. Catal. 236 (2005) 190.
[52] A. Gandubert, E. Krebs, C. Legens, D. Costa, D. Guillaume, P. Raybaud, Catal. Today 130 (2008) 149.
[53] Y. Zhao, R. Prins, J. Catal. 222 (2004) 532.